Liquid Crystals,
Vol. 35, No. 9, September 2008, 1061–1071

Taylor & Francis
Taylor & Francis Group

Calorimetric study of the isotropic to nematic phase transition in an aligned liquid crystal nano-colloidal gel

F. Crucenau[a], D. Liang[b], R. L. Leheny[b] and G. S. Iannacchione[a]*

[a]*Department of Physics, Worcester Polytechnic Institute, Worcester, MA 01609, USA;* [b]*Department of Physics and Astronomy, Johns Hopkins University, Baltimore, MD 21218, USA*

(Received 31 May 2008; final form 23 July 2008)

A high-resolution calorimetric study of the specific heat (C_p) has been carried out for the isotropic to nematic phase transition in an aligned liquid crystal (octylcyanobiphenyl - 8CB) and aerosil nano-colloid gel. A stable alignment was achieved by repeated thermal cycling of the samples in the presence of a strong uniform magnetic field, which introduces anisotropy to the quenched random disorder of the silica gel. In general, the specific heat features of the $I-N$ transition in aligned (anisotropic) gel samples are consistent with those seen in random (isotropic) gel samples, namely the observance of two C_p peaks and non-monotonic transition temperature shifts with increasing silica concentration. However, larger transition temperature shifts with silica density, modification of the phase conversion process in the two-phase coexistence region, and a larger effective transition enthalpy are observed for the aligned samples. The lower-temperature aligned C_p peak is larger and broader while exhibiting less dispersion than the equivalent peak for the random gel. This may be a consequence of the alignment altering the evolution from random-dilution-dominated to random-field-dominated effects. The exact origin of the larger transition temperature shifts is uncertain but the larger enthalpy suggests that the nematic state is different in the aligned system than in random gels. The general non-monotonic behaviour of the transition temperature is interpreted using dimensional analysis as a combination of an effective elastic stiffening of the liquid crystal combined with a liquid crystal and aerosil surface interaction energy.

Keywords: calorimetry; nematic; aerosil gel; quenched disorder

1. Introduction

Because of the wide range of physics involved, the study of quenched random disorder on phase structure and transitions is an important area that continues to attract extensive research activity. Here, the use of complex fluids or soft-systems in the presence of quenched random disorder has recently played a central role. In particular, progress has been made using liquid crystal (LC) as the host material and a variety of porous media or dispersed solids as the mechanism to introduce quenched random disorder (QRD).

One useful physical model is the LC+aerosil system where the QRD is created by a dispersed gel of silica aerosil particles that form a weakly linked gel and is varied by changing the density of aerosils in the dispersion. Numerous studies have previously been carried out by various groups on LC+aerosil (*1*) and the related LC+aerogel system (*2*), where aerogels are strongly linked (fused) silica gels. The most thoroughly studied LC+aerosil system is the dispersion of type-300 aerosil in octylcyanobiphenyl (8CB), denoted 8CB+sil. Detailed calorimetric (*3–5*), x-ray scattering (*6, 7*), x-ray intensity fluctuation spectroscopy (*8, 9*), static and dynamic light-scattering (*10–12*), and deuterium nuclear magnetic resonance (NMR) (*13*) studies on the nematic to smectic-*A* (*N*–Sm*A*) and the isotropic to nematic ($I-N$) phase transitions of this system have shown that there are clear quenched random-field characteristics as well as finite-size scaling effects (*1*).

The effect of the aerosil gel network on the orientational order of the nematic phase is two-fold. The silica gel firstly dilutes the LC and secondly creates a preferred local orientation (*14*). However, when the random gel responsible for the imposing of this random-field effect is strained, i.e. the gel takes on some anisotropy, a long-range ordered anisotropic nematic state is predicted (*15*). This is analogous to a similar situation for smectic ordering where disorder anisotropy may lead to an '*XY*-Bragg glass' phase (*16, 17*) as opposed to a smectic Bragg glass for isotropic disorder (*18, 19*). Experimental evidence supporting both predictions of anisotropic disorder has recently been found by a high-resolution x-ray study of smectic ordering in aligned 8CB+sil samples (*20*). The present calorimetric work is stimulated by the x-ray study but focuses on the $I-N$ transition of

*Corresponding author. Email: gsiannac@wpi.edu

ISSN 0267-8292 print/ISSN 1366-5855 online

DOI: 10.1080/02678290802372478
http://www.informaworld.com

aligned 8CB+sil. The results of a high-resolution calorimetric study on the smectic ordering in aligned 8CB+sil samples will be presented in a separate paper.

In this work, the effect of anisotropy is studied by calorimetry on the weakly first-order $I-N$ transition by preparing orientationally aligned 8CB+sil gels, denoted as **a**8CB+sil, and compared to unaligned, random, 8CB+sil samples, denoted as **r**8CB+sil. A convenient measure of the introduced disorder in these systems is the grams of silica per cm^3 of LC, denoted the conjugate silica density ρ_S, which is directly related to the surface area of solids as well as the mean distance between solid surfaces (*1, 4*). The units of ρ_S will be dropped hereafter. In general, the specific heat (C_p) signatures of the $I-N$ transition in **a**8CB+sil are found to be consistent with previous measurements on **r**8CB+sil samples (*1*). The anisotropy only subtly affects the shape of the $C_p(T)$ variation near the transition, where double specific heat peaks are signatures characteristic of LC+sil systems with $\rho_S \lesssim 0.1$. This double-peak feature can be understood as a cross-over from random-dilution-dominated to a random-field-dominated I to N phase conversion (*21*). Significant departures from the **r**8CB+sil results in a larger magnitude of the transition temperature shift and in the evolution of the effective transition enthalpy as a function of ρ_S for the **a**8CB+sil system. The counter-intuitive result of a *lower* T_{IN} for **a**8CB+sil despite having longer-range nematic order may be the result of larger nematic domains encompassing more disorder sites. The larger effective transition enthalpy and qualitatively different ρ_S dependence suggests that the nematic state for the aligned system is different than that in the random system.

An empirical modelling of the effective double-peak specific heat in the I+N coexistence region has been developed in order to extract the ρ_S dependence of the low- and high-temperature peaks. This analysis indicates that the low-temperature, random-field-dominated peak is essentially constant over the range of ρ_S studied while the high-temperature, random-dilution-dominated peak decays rapidly with increasing aerosil density, disappearing at $\rho_S \approx 0.13$. Finally, a dimensional analysis of the general non-monotonic transition temperature shift has been performed. The analysis yields a consistent scaling for a variety of disordering porous media and may indicate that the interplay of surface interaction energy and effective elasticity of the host fluid *within an ordered domain* is modified systematically by the colloidal dispersions.

Section 2 describes the preparation of the 8CB and aerosil dispersion samples in the random and aligned states as well as the ac-calorimetry technique employed. Section 3 presents an overview of the calorimetric results. These results are discussed in Section 4, with emphasis on the C_p doubling near the $I-N$ transition and the non-monotonic transition temperatures shifts as a function of ρ_S. The conclusions are summarized in Section 5.

2. Sample preparation and calorimetry

Nano-colloidal mixtures of the LC+sil samples were prepared using the solvent-dispersion method (*4*). The LC octylcyanobiphenyl (8CB, obtained from Frinton Laboratories Inc. and having a molar mass of $291.44\,g\,mol^{-1}$) and the hydrophilic type-300 aerosil (sil, obtained from DeGussa, Inc. having 7-nm diameter particles and $300\,m^2g^{-1}$ specific area) were prepared after thoroughly degassing at high temperature and under vacuum for at least 2 h. After dispersing measured amounts of 8CB and sil in high-purity (low-water) acetone, the solvent was allowed to evaporate slowly over several hours. The final mixture was then degassed at $\sim$320 K for 2–3 h to ensure complete removal of the acetone. Six different 8CB+sil batches were made with densities in the range $\rho_S = 0.030 - 0.150$. The resulting 8CB+sil has a dispersed aerosil gel structure that is fractal in character over a range of length scales (*4, 9*) and is termed here a random sample.

The aligned 8CB+sil, **a**8CB+sil, samples were achieved by thermally cycling a given mixture in a sealed calorimeter cell $\sim$100 times through the $I-N$ phase transition in the presence of a 2 T magnetic field. For $\rho_S \gg 0.1$, no significant alignment could be imposed. Two control random 8CB+sil, **r**8CB+sil, samples at $\rho_S = 0.050$ and 0.130 were also made from the same batch of 8CB and they experienced the exact same thermal history except with no aligning magnetic field present. In the presence of a magnetic field, the nematic director of 8CB tends to align parallel to the field, and this tendency competes with the quenched random disorder of the gel. Due to the elasticity of the LC and the compliance of the gel, this competition leads to restructuring of the gel to accommodate the magnetic anisotropy. As a result, the quenched disorder becomes no longer random but on average orients nematic domains along the direction of the applied field. After removal of the field and subsequent temperature cycling, the aligned structure of the gels continues to promote macroscopic long-range order of the nematic, with a narrow distribution of director orientations as evidenced by x-ray studies on nearly identically prepared samples (*20, 22*). The x-ray studies also found that the aerosil gel scattering was nearly independent of the alignment procedure, indicating that the alignment is

maintained by a rearrangement of the aerosil gel on very long length scales and the gel remains random locally (*22*). It may be expected then that the large length scales of nematic (director) ordering would be affected by the alignment, which is the focus of this work.

High-resolution ac-calorimetry was performed using a home-built calorimeter whose basic characteristics have been described elsewhere (*23*). The technique consists of applying heating power to the cell as $P_{ac}e^{i\omega t}$ and detecting the resulting temperature oscillations having an amplitude T_{ac} and a relative phase shift of $\varphi \equiv \Phi + \pi/2$, where Φ is the absolute phase shift between $T_{ac}(\omega)$ and the input power. The specific heat at a heating frequency ω is given by

$$C_p = \frac{\left[C'_{filled} - C_{empty}\right]}{m_{sample}} = \frac{P_{ac}\cos\varphi/\omega|T_{ac}| - C_{empty}}{m_{sample}}, \quad (1)$$

$$C''_{filled} = \frac{P_{ac}}{\omega|T_{ac}|}\sin\varphi - \frac{1}{\omega R}, \quad (2)$$

where C'_{filled} and C''_{filled} are the real and imaginary components of the heat capacity, C_{empty} is the heat capacity of the cell and silica, m_{sample} is the mass in grams of the LC (the total mass of the 8CB+sil sample was $\sim$15 mg, which yielded m_{sample} values in the range 10–15 mg), and R is the thermal resistance between the cell and the bath (typically 200 K W^{-1}). Equations (1) and (2) require a small correction to account for the finite internal thermal resistance compared to R, and this was applied to all samples studied here (*24*). Measurements were conducted at various frequencies in order to ensure the applicability of Equations (1) and (2) by checking that $C''_{filled} \approx 0$ through the effective N–SmA transition at T^* and that C_p was independent of ω. All data presented here were taken at $\omega = 0.1473\,\mathrm{s}^{-1}$ at a scanning rate of less than ± 200 mK h^{-1}, which yielded essentially static C_p results. All 8CB+sil samples experienced the same thermal history after mounting; 6 h in the isotropic phase to ensure equilibrium, then a slow cool deep into the smectic phase before beginning the first detailed scan upon heating.

Extraction of the enthalpy behaviour involves integrating the excess specific heat $\Delta C_p = C_p - C_{BG} - \delta C_{NA}$, where C_{BG} is a linear background describing the specific heat temperature dependence far above (+6 K) and below (-13 K) T_{IN} and δC_{NA} is the N–SmA excess specific heat contribution. Note that the high-temperature limit of the two-phase I+N coexistence range, easily identified in C''_p, is taken as T_{IN}. Direct integration of ΔC_p yields δH^*_{IN}, which contains only a portion of the transition latent heat (*4*). Replacing the ΔC_p behaviour in the I+N coexistence region with a linear extrapolation between the boundary points as in (*4*) and then integrating yields the fluctuation dominated 'wing' enthalpy δH_{IN}. The difference $H = \delta H^*_{IN} - \delta H_{IN}$ is the effective phase conversion enthalpy observed by ac-calorimetry. In this study, the 19 K range of integration, temperature scan rates, heating frequency and sample thermal history were all the same for all samples in order to facilitate comparisons. However, due to uncertainties in background subtractions, the absolute accuracy in δH^*_{IN} is about 10%.

3. Results

An expanded view of the excess specific heats for the aligned and random 8CB+sil samples along with pure bulk 8CB from -12 K below to +5 K above the $I-N$ transition are shown in Figure 1. Here, we take as the transition temperature the high-temperature point where $C''_p \neq 0$, i.e. the high-temperature limit of the I+N coexistence. The excellent overlap of ΔC_p in the isotropic and smectic-A phases is consistent with previous measurements on the (random) 8CB+sil

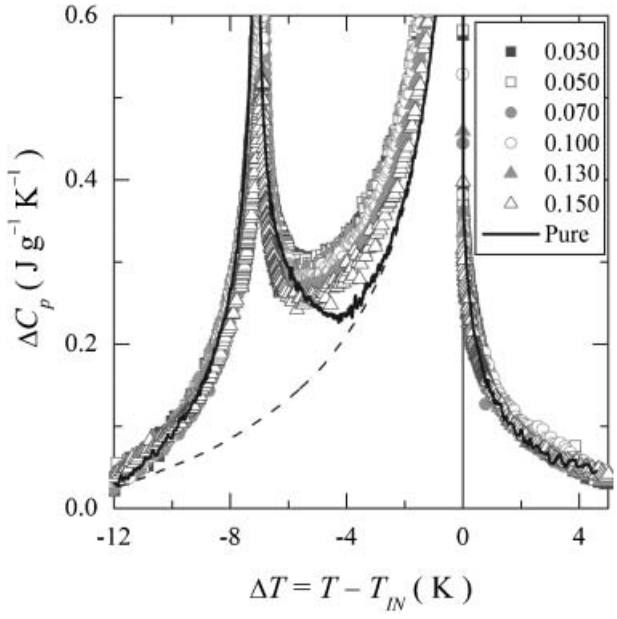

Figure 1. Expanded view of the excess specific heat over a wide temperature range about the I+N transition for the six **a**8CB+sil samples and bulk 8CB. The ρ_S values are given in the inset. Note the excellent overlap in the isotropic and smectic-A phases for all samples while significant excess enthalpy is seen in the nematic phase for the **a**8CB+sil samples.

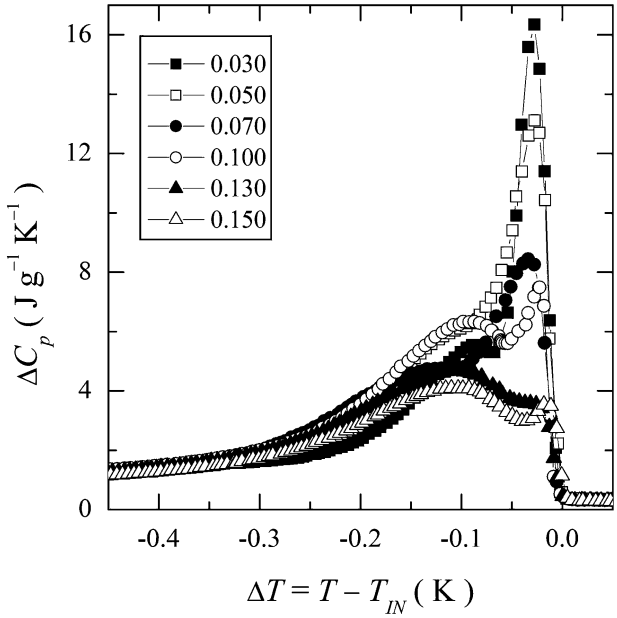

Figure 2. Overview of the excess specific heat over the two-phase I+N coexistence region of the $I-N$ phase transition for the **a**8CB+sil samples. The inset denotes the symbols for the ρ_S values of the six samples. Note that the transition temperature T_{IN} is taken as the high-temperature limit of the coexistence region.

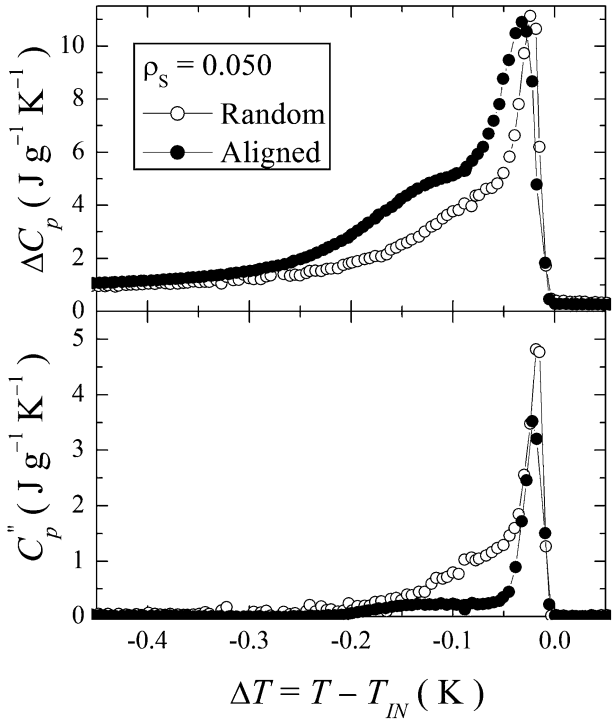

Figure 3. Comparison of the real excess specific heat, ΔC_p, and imaginary (dispersive) specific heat, C_p'', for the aligned and unaligned random ρ_S=0.050 8CB+sil sample as a function of temperature near T_{IN}. Note the broadening and enhancement of the low-temperature $\Delta C_p'$ peak along with a suppression of its dispersive nature for the aligned compared to the random sample.

system (*4*) indicating that the anisotropy imposed by the alignment does not affect the short-range orientational fluctuations and that these remain bulk-like independent of the aerosil structure. However, large differences are seen in the nematic temperature range where there is clearly an excess of enthalpy. This excess generally decreases with increasing ρ_S and approaches the bulk curve.

Figure 2 provides an overlay of ΔC_p for the six **a**8CB+sil samples studied near and about the $I-N$ coexistence region. As with the random sil system, a double-peak feature is clearly seen and this is currently understood to be marking the crossover from random-dilution-dominated to random-field-dominated disorder (*21*). In addition, a dramatic suppression of the dilution-dominated sharper, high-temperature ΔC_p is also seen in the aligned samples for $\rho_S \geqslant 0.100$, marking the boundary between the soft and stiff gel regime (*4*).

To highlight the effect of alignment, two samples from the same mixture batch at low and high ρ_S were also studied without any field alignment (random) but experiencing identical experimental conditions. Comparisons between the random and aligned samples are shown in Figure 3 for the ρ_S=0.050 and Figure 4 for the ρ_S=0.130 samples. For the low density sample, alignment appears to broaden and enhance both ΔC_p transition peaks but the width of coexistence is unchanged. Also, the imaginary part indicates that the lower-temperature, random-field-dominated peak is less dispersive. For the higher density sample, the excess specific heat is somewhat broadened but is essentially unchanged by the alignment as is the coexistence range. As with the low-density comparison, the dispersive nature of the low-temperature peak is suppressed by the alignment.

In both cases, the imaginary enthalpy (integrated area under C_p'') is smaller for the aligned as compared to the random samples. The real effective enthalpy δH_{IN}^* over a wide temperature range is larger for the **a**8CB+sil samples, due primarily to the excess heat capacity seen throughout the nematic temperature range. See Figure 5. This is in contrast to that seen in the previous 8CB+sil results where the heat capacity wings far away from T_{IN} overlapped each other and that of bulk 8CB. For the two **r**8CB+sil samples studied here, the wings yield an ρ_S-independent enthalpic contribution δH_{IN}=5.5 J g^{-1}, consistent with previous measurements on unaligned 8CB+sil samples (*4*). Also seen in Figure 5, the evolution of δH_{IN}^* for the **a**8CB+sil system appears to join that for the **r**8CB+sil system for ρ_S=0.150.

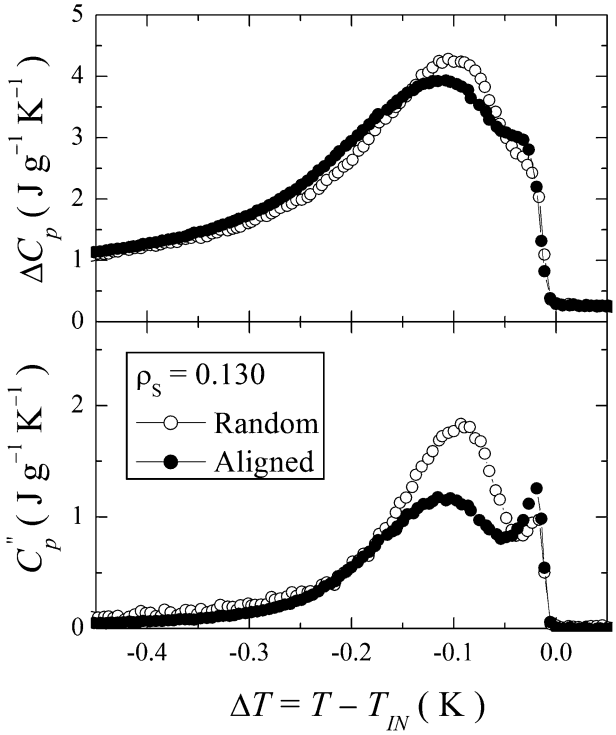

Figure 4. Comparison of the real excess specific heat, ΔC_p, and imaginary (dispersive) specific heat, C_p'', for the aligned and unaligned random ρ_S=0.130 8CB+sil sample as a function of temperature near T_{IN}. Note the slight broadening of the low-temperature $\Delta C_p'$ peak along with a partial suppression of its dispersive nature for the aligned compared to the random sample.

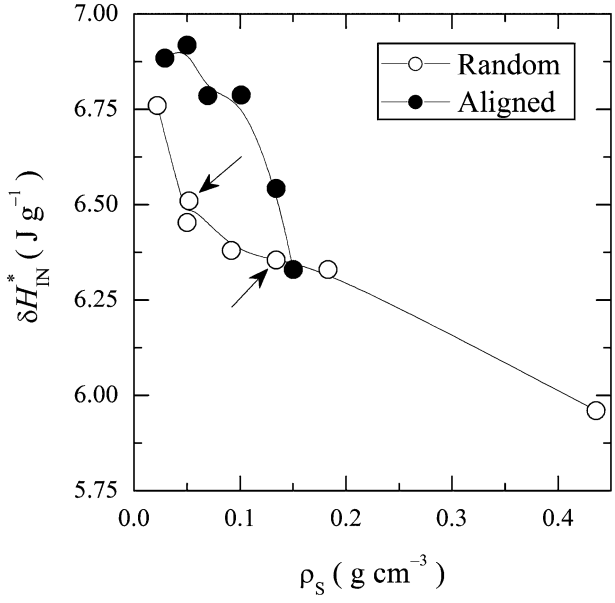

Figure 5. Effective integrated enthalpy δH^*_{IN} for the aligned (solid circles) and unaligned random (open circles, the latter from (*4*) plus two from this study indicated by the arrows) 8CB+sil samples as a function of ρ_S. These values were obtained by integrating $\Delta C_p(ac)$ from -13 K below to +6 K above T_{IN} with subtraction of the N–SmA contribution (*4*). Due to ambiguities in the choice of backgrounds, the absolute uncertainties are ~10% but the relative precision is higher (~3%).

While the excess specific heat is slightly altered by alignment, a more dramatic effect is seen in the behaviour of the transition temperatures. Qualitatively, the $I-N$ transition shifts to lower temperature as ρ_S increases in a similar manner as for the random samples. However, for all aligned samples, the magnitude of the shift with respect to the pure bulk value $\Delta T_{IN} = T_{IN}^{bulk} - T_{IN}(\rho_S)$ is ~0.5 K *larger*; see Figure 6. A comparison of the width of the nematic temperature range $\Delta T_{nem} = T_{IN} - T^*_{NA}$, shown in Figure 7 for the aligned and random samples, reveals that ΔT_{nem} for aligned samples is ~0.2 K less than for bulk 8CB while ΔT_{nem} for unaligned samples is essentially independent of ρ_S in the range of values studied here. Finally, the isotropic plus nematic coexistence range δT_{I+N}, determined by the temperature width of $C_p'' \neq 0$, for the aligned samples is essentially identical to that for random samples as seen in Figure 8.

It is important to note that sample degradation due to the repeated thermal cycling during sample preparation can be ruled out as the cause of the larger transition shifts for the aligned compared to the

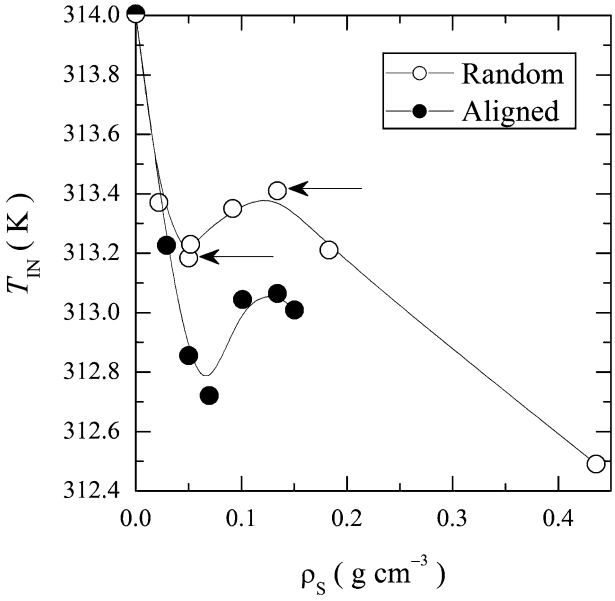

Figure 6. The isotropic to nematic phase transition temperature T_{IN} for the aligned and unaligned random (the latter from (*4*) plus two from this study indicated by the arrows) 8CB+sil samples as a function of ρ_S. The uncertainties in T_{IN}, taken as the lowest stable isotropic temperature, is ≈6 mK. Note the similar dependence but larger shift with ρ_S for aligned samples.

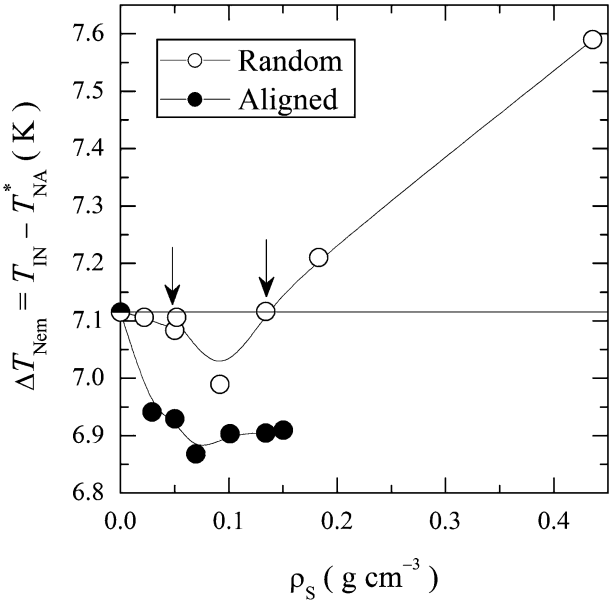

Figure 7. The nematic temperature range, $\Delta T_{nem} = T_{IN} - T^*_{NA}$, for the aligned and unaligned random (the latter from (*4*) plus two from this study indicated by the arrows) 8CB+sil samples as a function of ρ_S. Note the narrowing of ΔT_{Nem} for the aligned samples.

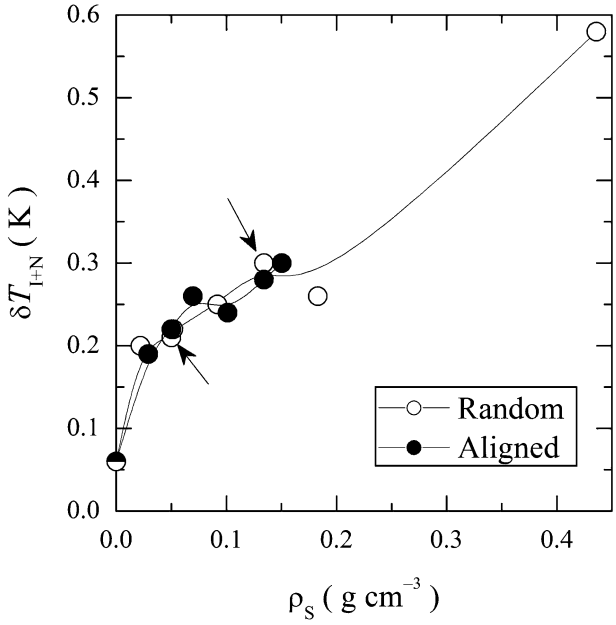

Figure 8. The isotropic plus nematic coexistence temperature range, δT_{I+N}, for the aligned and unaligned random (the latter from (*4*) plus two from this study indicated by the arrows) 8CB+sil samples as a function of ρ_S. As determined by the width of the dispersion (imaginary) C''_p peak, δT_{I+N} has an uncertainty of ~20 mK. Note that the coexistence width is insensitive to the alignment.

random 8CB+sil samples. The LC 8CB is known to be a stable compound when properly degassed and hermetically isolated as done in these calorimetric cells. Also, the coexistence width δT_{I+N}, which should be sensitive to the quality of the LC, appears to be unaffected by the sample preparation when compared to previous, more gently treated, measurements. See Figure 8. More convincingly, the control random samples measured in this study were subjected to identical thermal histories as were the aligned samples but nevertheless display smaller transition temperature shifts that are essentially identical to those measured for **r**8CB+sil samples in previous studies (*4*).

If the alignment is imprinted on the aerosil gel only on long length scales (*22*) and the local aerosil gel distribution remains unchanged, than the larger transition temperature shifts for the aligned samples may be the result of the larger nematic domains encompassing more aerosil gel (disorder). Additionally, the rearrangement of the aerosil gel for the aligned samples may also result in a stiffer gel as compared to the equivalent random, unaligned, gel and contribute to a larger ΔT_{IN}. Table 1 summarizes the transition temperatures, nematic temperature range, width of the two-phase coexistence and the effective enthalpy for the $I-N$ transition in six aligned and two random 8CB+sil samples studied.

4. Discussion

4.1. *Partitioning of the I−N double-C_p peak*

The most striking effect of an aerosil gel on the $I-N$ transition for both the aligned and unaligned (random) samples is the appearance of two closely spaced, transition features (*4, 5, 21, 25–30*). This

Table 1. Summary of the calorimetric results on the isotropic to nematic phase transition for the six aligned and two unaligned 8CB+sil samples. The units for conjugate aerosil density ρ_S are grams of aerosil per cm^3 8CB; the transition temperature T_{IN}, nematic range ΔT_{Nem} and coexistence width δT_{I+N} are in Kelvin; the effective acenthalpy δH^*_{IN} and the contribution of the high-temperature peak h_1 and low-temperature peak h_2 effective enthalpies are in Joules per gram 8CB (see the text for details). For all parameters, the uncertainties are ± 2 in the last digit except for δH^*_{IN}, which is ± 0.07, and the effective enthalpies h_1 and h_2, where it is ~10%.

Sample	ρ_S	T_{IN}	ΔT_{Nem}	δT_{I+N}	δH^*_{IN}	h_1	h_2
Aligned	0.030	313.226	6.941	0.19	6.88	0.62	0.83
	0.050	312.855	6.929	0.22	6.92	0.39	0.80
	0.070	312.721	6.870	0.26	6.78	0.24	0.74
	0.100	313.044	6.903	0.24	6.79	0.09	0.78
	0.130	313.064	6.904	0.28	6.54	0.01	0.88
	0.150	313.009	6.909	0.30	6.33	0.03	0.79
Unaligned	0.050	313.184	7.038	0.21	6.45	0.34	0.78
	0.130	313.410	7.116	0.30	6.36	0.12	0.90

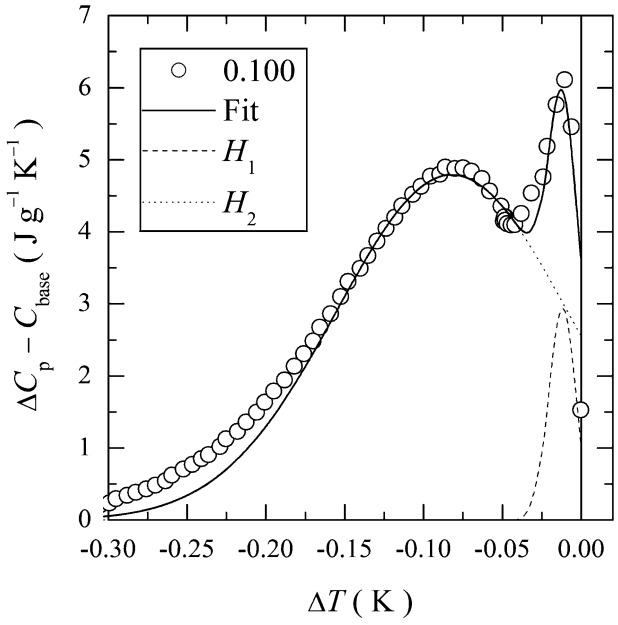

Figure 9. Fit (solid line) using a two-Gaussian form to model the excess specific heat over the entire two-phase (*I*+*N*) coexistence region of the ρ_S=0.100 aligned 8CB+sil sample. Dashed and dotted lines indicate the contributions of the high-temperature (H_1) and low-temperature (H_2) peaks, respectively. See inset. Note that the fit must be truncated at the high-temperature limit of the coexistence region and that a constant baseline value was subtracted. Fits made to the other samples were of similar quality.

effect is especially pronounced in the heat capacity data. This phenomena is understood to be a consequence of these soft-systems exhibiting a temperature-dependent disorder strength near the transition, which results in a crossover from random-dilution to random-field effects (*21*). The results of the present study are completely consistent with the literature for random gels and indicate only minor modification to the distribution of dilution and field effects for aligned samples.

To empirically partition the enthalpic contributions between the high-temperature, dilution dominated, and the lower-temperature, random-field dominated, $I-N$ C_p peaks, a simple double-Gaussian fit was performed only over the two-phase coexistence region. This ansatz must be truncated at the high-temperature limit of the coexistence region.

It is important to note that this approach *does not* represent any theory but only the *simplest* means of partitioning the enthalpy between the random-dilution and random-field effects. In addition, the integration of the ac-determined ΔC_p would yield only an effective enthalpy that includes part but not all of the first-order latent heat (see Section 2 and (*4*)). However, all measurements in this study were conducted under identical experimental conditions, and thus the effect of both alignment and aerosil density should be isolated by this analysis as a proxy for a more detailed experimental measurement of the true total transition enthalpy.

An example of such a double-Gaussian modelling of the ΔC_p data through the *I*+*N* coexistence region is shown in Figure 9. Similar quality fits were obtained for all aligned and random samples studied. From these fit results, the area for each contribution (each truncated at the high-temperature limit of the coexistence range) H_1 and H_2, respectively, can be extracted. However, as seen in Figure 9 and similarly for all such fits, this approach clearly is inadequate to quantitatively model the peak farther than about 0.2 K from T_{IN} and so the total integration would not yield the correct H as obtained experimentally. By assuming that the ratio of each term's area, $R \equiv H_1/H_2$ is close to being correct and taking the measured H, a reasonable estimate of each peak's area may be calculated by $h_1 = RH/(1+R)$ and $h_2 = H/(1+R)$ for the high- and low-temperature peaks, respectively (with $h_1+h_2 \equiv H$). The uncertainties in h_1 and h_2, which are $\sim$10%, are due to the quality of the fit while the uncertainty in H is typically $\pm 0.05\,\mathrm{J\,g^{-1}}$. These results are listed in Table 1 for all of the samples studied. Comparison of the h_1 and h_2 contributions for the random and aligned samples with ρ_S=0.050 indicates that, despite the obvious broadening seen in Figure 3 for the aligned sample, the relative contributions of dilution and field effects remain unchanged. However, for the sample with ρ_S=0.130, there is a significant increase in the random-dilution contribution to the transition enthalpy for the aligned sample.

Plots of the ρ_S dependence of the peak areas h_1 and h_2 are shown in Figure 10. The low-temperature, random-field-dominated, effective enthalpy h_2 is effectively constant through this low range of aerosil densities, while the high-temperature, random-dilution-dominated, effective enthalpy h_1 decreases rapidly with ρ_S, mirroring the decrease of the total effective enthalpy H, until it essentially vanishes at $\rho_S \approx 0.13$. Although this can be inferred from the behaviour shown in Figure 2, this analysis makes it clear that the decrease in the $I-N$ transition enthalpy occurs in two stages. In the low-density range ($\rho_S \leqslant 0.1$), the random-dilution-dominated peak decays, while the random-field-dominated peak is nearly ρ_S independent. Given the results of the wider ρ_S range studies of (*4*) and (*26*), the remaining random-field-dominated peak should begin to decrease for larger ρ_S and eventually disappear at $\rho_S \approx 0.8$. Such a scenario, coupled with the temperature-dependent total disorder strength of the random dilution to random field crossover (*21*), may be

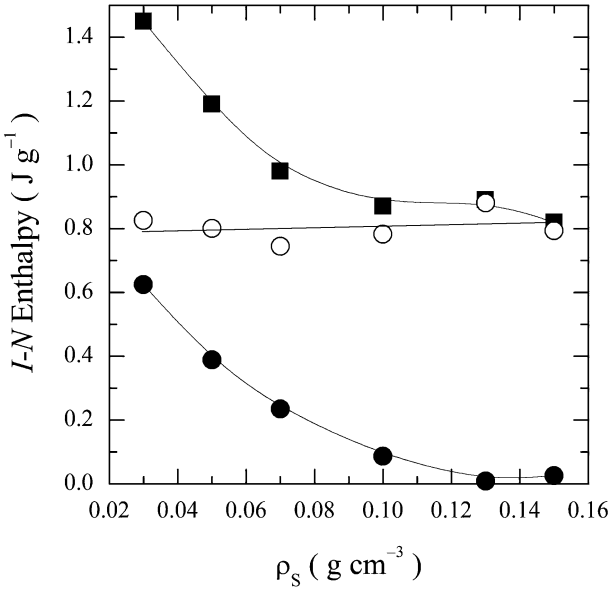

Figure 10. Plot of the ρ_S dependence of the random-dilution-dominated, high-temperature peak enthalpy h_1 (solid circles), the random-field-dominated, low-temperature peak enthalpy h_2 (open circles) and the measured coexistence area H (solid squares) for the aligned 8CB+sil samples. The solid lines are guides to the eye. Note the near constant behaviour of h_2 in contrast to the rapid decrease in h_1.

important in explaining the non-monotonic transition temperature decrease with ρ_S.

4.2. *Dimensional analysis: ΔT_{IN}*

A striking effect of the aerosil gel on the $I-N$ transition is the non-monotonic shift in the transition temperature, ΔT_{IN}, as shown in Figure 6. The first-order transition temperature typically shifts as a function of impurities, such as solvents, and it has been extensively studied (*31–33*). However, the aerosil gel here imposes quenched random disorder leading to additional interactions other than dilution that dominates in LC and solvent mixtures.

Various mechanisms have been explored to account for the observed transition temperature shift behaviour in LC+sils such as finite-size nucleation (due to the first-order character of the $I-N$ transition), elastic strain, random pinning (see (*4, 34*) for a discussion of these three), and more recently an extended 'single-pore' model to account for surface anchoring (*35*). However, all current models yield smoothly varying functions of confining length or disorder (silica) density and the non-monotonic behaviour remains unexplained. Recently, it has been shown that the $I-N$ transition in the presence of quenched random disorder proceeds via a two-step process on cooling, first random-dilution and then random-field, and this successfully accounts for the doubling of the $I-N$ transition features (*21*). Further, it was speculated that this might also account for the behaviour of ΔT_{IN} for these systems via the required temperature-dependent disorder strength (see also (*27*)) but this idea remains unexplored.

Other experimental observations on the LC+sil system as a function of ρ_S, such as the evolution of the critical behaviour of the N–SmA (*4, 20, 28*) and ΔC_P peak shape of the SmA–SmC (*30*) transitions, rheological studies (*36*) and dynamic x-ray scattering studies (*8, 9*), strongly suggest that the colloidal dispersion of the aerosil gel alters the effective elastic (and perhaps other material) properties of the host LC fluid.

To explore the idea that the LC material parameters may become ρ_S dependent, a dimensional analysis may be performed on ΔT_c based on four important quantities: the effective elastic constant of the composite, $\bar{K}$ in (J m^{-1}), the effective surface interaction energy density, W in (J m^{-2}), the conjugate aerosil density, ρ_S in (kg m^{-3}) and the transition entropy change, ΔS_c in (J K^{-1} kg^{-1}), yielding

$$|\Delta T_c| \sim \frac{W^2}{\bar{K}\rho_S \Delta S_c} \sim \frac{W^2 T_c}{\bar{K}\rho_S \Delta H_c}, \qquad (3)$$

where the entropy change at T_c is related to the enthalpy change (latent heat) by $\Delta H_c = T_c \Delta S_c$. Note that if the bulk value of $\bar{K}$ as well as the anchoring energy density W were assumed constant, Equation (3) would also not yield the observed non-monotonic behaviour of ΔT_c. However, if $\bar{K}$ and W were aerosil dependent, then this analysis could be used to shed light on the ρ_S dependence of the effective material parameters of the composite system. A ρ_S-dependent $\bar{K}$ is clear given that aerosils are used as thickeners and a ρ_S-dependent W is reasonable given the flexibility of the aerosil gels (*9*). However, for other systems such as LCs embedded in rigid aerogel or controlled porous glasses, it is more natural to consider W as a constant. Equation (3) may be rearranged to group together the experimentally accessible quantities to give

$$\frac{|\Delta T_c|}{T_c} \Delta H_c \rho_S \sim \frac{W^2}{\bar{K}}, \qquad (4)$$

which has units of (J m^{-3}) and can be termed the LC+QRD energy density. Accurate ac-calorimetric data are available for the LC 8CB in controlled porous glass (*35*), aerogel (*37*), random aerosil gel

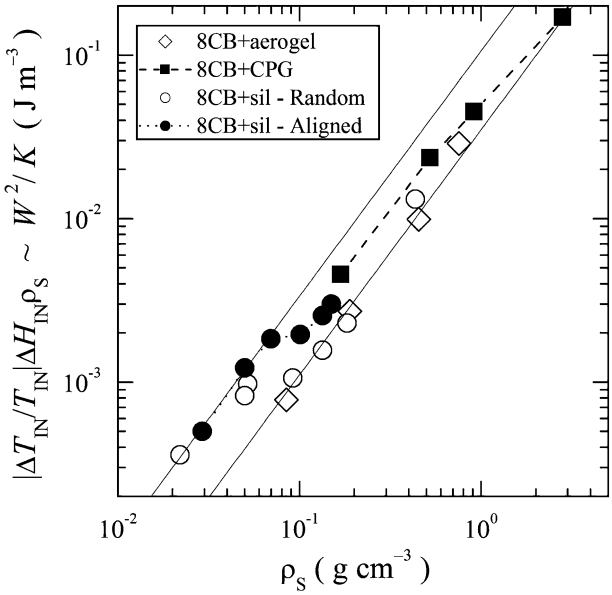

Figure 11. Comparison of the derived LC+QRD energy density $W^2/\bar{K}$ as a function of ρ_S for the 8CB+QRD (8CB+aerogel (*37*), 8CB+CPG (*35*), random 8CB+sil (*4*) with two points from this work and the aligned 8CB+sil (this work)). See the inset for symbol labels. Both solid lines indicate a power law with an exponent of $n=1.5$. See the text for details.

(*4*) and the aligned aerosil gel of this work. However, each data set, although taken under similar ac-calorimetric experimental conditions, is missing a significant portion of the latent heat. Thus, the effective transitional enthalpy available from these studies are used only as a proxy for the true value of ΔH_{IN}.

With Equation (4), the ρ_S dependence of the combination $W^2/\bar{K}$ is found and plotted in Figure 11. Given the uncertainties (primarily in estimating ΔH_{IN} from δH_{IN}^*), the data collapse for such a range of 8CB+QRD systems is interesting and somewhat surprising. The overall behaviour of the LC+QRD energy density is reasonably describable by a simple power law, $W^2/K \sim \rho_S^n$ where the exponent for the low-density ($\rho_S<0.1$) aerosil system and the high-density ($\rho_S>0.1$) aerosil along with the aerogel systems is $n=1.5$ (see the solid lines in Figure 11). Since the low-density aerosil gel is extremely soft as compared to the aerogel (or controlled porous glass or high-density aerosil), the dimensional analysis suggests that the non-monotonic behaviour of $T_{IN}(\rho_S)$ may reflect a change in the effective stiffness and/or anchoring of the LC to the QRD surfaces occurring over a very narrow range at or just above $\rho_S \sim 0.10$, where $W^2/\bar{K}$ shifts between the two solid parallel lines in Figure 11.

Given the overall behaviour of the LC+QRD energy density, the functional dependence of W and $\bar{K}$ separately may be inferred for soft-systems such as low-density aerosil gels. Using the observed power law and the condition that as $\rho_S \to 0$, $W \to 0$ (no surfaces present) and $\bar{K} \to \bar{K}_0$ (the bare bulk LC value), this suggests $W \sim \rho_S^w$ and $K \sim K_0 + c\rho_S^k$. Noting that the exponents n, w and k must be positive, a relationship among them depends on the magnitude of $\bar{K}_0$ relative to the diverging part. If $\bar{K}_0$ is negligibly small, then the exponents must satisfy $2w-k=n>0$. Otherwise, the general relation $2w-k<n<2w$ applies. Overall, this result is intuitively reasonable as the random nature of the solid surfaces causes them to trap more disorder energy as the solid density increases. However, an increasing $\bar{K}$ with increasing ρ_S, i.e. $c>0$, assumes that the composite effectively stiffens the host LC by the pinning defects and domain walls. This analysis also allows for the possibility that $\bar{K}$ decreases with increasing ρ_S, i.e. $c<0$ with a large $\bar{K}_0$, and this would represent an elastic softening of the LC due to the imposed disorder.

For rigid quenched random disorder where W is likely to be constant dependent only on surface interactions, the above analysis would not hold. For such systems, these results would only shed insight into the overall behaviour of $W^2/\bar{K}$.

5. Conclusions

This work presents a high-resolution calorimetric study of the effect of sil alignment on the isotropic to nematic phase transition of the quenched disordered 8CB+aerosil system. As expected, the overall specific heat signature of the $I-N$ transition in this system is weakly affected by the alignment, reflecting the scalar nature of the energy fluctuations. The results are largely consistent with results on unaligned (random gel) samples, again revealing as the most significant features the doubling of the $I-N$ transition and a non-monotonic decrease in the transition temperature with aerosil density. Thus, the imposition of long-range orientational order does not significantly change the transition characteristics. However, differences do emerge in the magnitude of the transition temperature shift, with the shift being unexpectedly larger for the aligned disorder, and there being small changes in the C_p peak shapes in the coexistence range and significant excess enthalpy throughout the nematic temperature range. How the sil alignment causes these effects is not entirely clear but it may be related to the aligned samples having larger nematic domains and so being forced to encompass more aerosil surface (disorder). In addition, there is the possibility that the aligned aerosil gel may be stiffer than the random gel and so impose

greater disorder. The latter observation strongly indicates that the nematic state in the aligned samples differs significantly from that in the random samples.

An empirical analysis of the specific heat peak shapes using a two-Gaussian model yields a reasonably accurate partitioning of the effective enthalpy between the dilution-dominated and field-dominated peaks. While not containing any theoretical insights into the disorder, the decent fits indicate the normal distribution of the isotropic to nematic phase conversion under the influence of random-dilution and random-field effects with relatively little coupling. In addition, the aerosil density dependence indicates that the random-field-dominated peak h_2 is nearly constant from the percolation threshold ($\rho_S \sim 0.015$) to $\rho_S = 0.15$, while the random-dilution-dominated peak h_1 decays rapidly. This analysis combined with the results of (*4*) and (*26*) indicates that the decrease in the $I-N$ transition enthalpy H determined from $C_p(ac)$ data (and presumably the total latent heat as well) occurs in two stages. As ρ_S increases, there is a rapid decrease in the random-dilution-dominated contribution, which disappears at $\rho_S \cong 0.13$, and this is followed by an eventual decrease in the random-field-dominated contribution when the aerosil density is increased above 0.15.

A dimensional analysis of the transition temperature shifts as a function of aerosil density resulted in a relationship that involves an effective elastic constant as well as a surface interaction energy. This analysis further suggests that both these quantities behave as power laws with aerosil density. In addition, the same analysis applied to a variety of 8CB systems with quenched random disorder, such as unaligned (random) aerosil gels, aerogel gels and controlled-porous glasses, reveals a general behaviour and indicates that the resulting exponents are topology independent. High-resolution latent heat measurements through the double-peak feature would greatly aid the peak partition analysis as well as better refine the LC+QRD energy density estimate. Finally, since the origin of the imprinted alignment is undoubtedly a rearrangement of the aerosil gel structure, it would be extremely useful to have a detailed structural study, such as small-angle x-ray scattering, of the aerosil gel under varying degrees of alignment.

Acknowledgements

We wish to thank C. W. Garland and T. Bellini for many useful discussions. This work was supported at WPI by the NSF under Grant No. DMR-0092786 and at Johns Hopkins by NSF under Grant No. DMR-0134377.

References

(1) Iannacchione G.S.; Park S.; Garland C.W.; Birgeneau R.J.; Leheny R.L. *Phys. Rev. E* **2003**, *67*, 011709–13.
(2) Bellini T.; Radzihovsky L.; Toner J.; Clark N.A. *Science* **2001**, *294*, 1074–1079.
(3) Zhou B.; Iannacchione G.S.; Garland C.W.; Bellini T. *Phys. Rev. E* **1997**, *55*, 2962–2968.
(4) Iannacchione G.S.; Garland C.W.; Mang J.T.; Rieker T.P. *Phys. Rev. E* **1998**, *58*, 5966–5981.
(5) Marinelli M.; Ghosh A.K.; Mercuri F. *Phys. Rev. E* **2001**, *63*, 061713–9.
(6) Park S.; Leheny R.L.; Birgeneau R.J.; Gallani J.-L.; Garland C.W.; Iannacchione G.S. *Phys. Rev. E* **2002**, *65*, 050703(R).
(7) Leheny R.L.; Park S.; Birgeneau R.J.; Gallani J.L.; Garland C.W.; Iannacchione G.S. *Phys. Rev. E* **2003**, *67*, 011708–13.
(8) Retsch C.; McNulty I.; Iannacchione G.S. *Phys. Rev. E* **2002**, *65*, 032701–4.
(9) Roshi A.; Barjami S.; Iannacchione G.S.; Paterson D.; McNulty I. *Phys. Rev. E* **2006**, *74*, 031404.
(10) Bellini T.; Clark N.A.; Degiorgio V.; Mantegazza F.; Natale G. *Phys. Rev. E* **1998**, *57*, 2996–3006.
(11) Bellini T.; Buscaglia M.; Chiccoli C.; Mantegazza F.; Pasini P.; Zannoni C. *Phys. Rev. Lett.* **2000**, *85*, 1008–1011.
(12) Bellini T.; Buscaglia M.; Chiccoli C.; Mantegazza F.; Pasini P.; Zannoni C. *Phys. Rev. Lett.* **2002**, *88*, 245506–4.
(13) Jin T.; Finotello D. *Phys. Rev. Lett.* **2001**, *86*, 818–821.
(14) Gingras M.J.P. *Ordering of liquid-crystals in porous media* **1995**, private communication.
(15) Feldman D.E. *Phys. Rev. Lett.* **2000**, *84*, 4886–4889.
(16) Jacobsen B.; Saunders K.; Radzihovsky L.; Toner J. *Phys. Rev. Lett.* **1999**, *83*, 1363–1366.
(17) Saunders K.; Jacobsen B.; Radzihovsky L. *J. Toner, J. Phys.: Condens. Matter* **2000**, *12*, A215–A220.
(18) Radzihovsky L.; Toner J. *Phys. Rev. Lett.* **1997**, *79*, 4214–4217.
(19) Radzihovsky L.; Toner J. *Phys. Rev. B* **1999**, *60*, 206–257.
(20) Liang D.; Leheny R.L. *Phys. Rev. E* **2007**, *75*, 031705.
(21) Caggioni M.; Roshi A.; Barjami S.; Mantegazza F.; Iannacchione G.S.; Bellinil T. *Phys. Rev. Lett.* **2004**, *93*, 127801–127804.
(22) Liang D.; Borthwick M.A.; Leheny R.L. *J. Phys.: Condens. Matt.* **2004**, *16*, S1989–2002.
(23) Yao H.; Garland C.W. *Rev. Sci. Instrum.* **1998**, *69*, 172–178.
(24) Sharma D.; Iannacchione G.S. *J. Chem. Phys.* **2007**, *126*, 094503.
(25) Hourri A.; Bose T.K.; Thoen J. *Phys. Rev. E* **2001**, *63*, 051702.
(26) Jamee P.; Pitsi G.; Thoen J. *Phys. Rev. E* **2002**, *66*, 021707–8.
(27) Clegg P.S.; Stock C.; Birgeneau R.J.; Garland C.W.; Roshi A.; Iannacchione G.S. *Phys. Rev. E* **2003**, *67*, 021703.
(28) Roshi A.; Iannacchione G.S.; Clegg P.S.; Birgeneau R.J. *Phys. Rev. E* **2004**, *69*, 031703–14.
(29) Jin T.; Finotello D. *Phys. Rev. E* **2004**, *69*, 041704.
(30) Roshi A.; Iannacchione G.S.; Clegg P.S.; Birgeneau R.J.; Neubert M.E. *Phys. Rev. E* **2005**, *72*, 051716.
(31) Oweimreen G.A.; Martire D.E. *J. Chem. Phys.* **1980**, *72*, 2500–2510.

(32) Matsuyama A.; Evans R.M.L.; Cates M.E. *Phys. Rev. E* **2000**, *61*, 2977–2986.
(33) Matsuyamaa A.; Hirashima R. *J. Chem. Phys.* **2008**, *128*, 044907–11.
(34) Iannacchione G.; Finotello D. *Phys. Rev. E* **1994**, *50*, 4780–4795.
(35) Kutnjak Z.; Kralj S.; Lahajnar G.; Žumer S. *Phys. Rev. E* **2003**, *68*, 021705.
(36) Bandyopadhyay R.; Liang D.; Colby R.H.; Harden J.L.; Leheny R.L. *Phys. Rev. Lett.* **2005**, *94*, 107801.
(37) Wu L.; Zhou B.; Garland C.W.; Bellini T.; Schaefer D.W. *Phys. Rev. E* **1995**, *51*, 2157–2165.